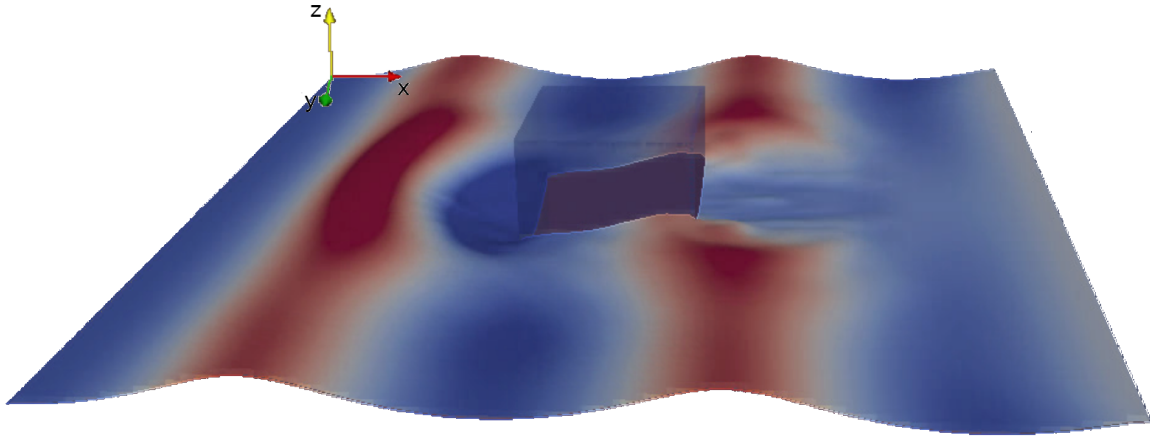


Graphical Abstract

Optimizing wave-generation and wave-damping in 3D-flow simulations with implicit relaxation-zones

Robinson Perić, Vuko Vukčević, Moustafa Abdel-Maksoud, Hrvoje Jasak



Highlights

Optimizing wave-generation and wave-damping in 3D-flow simulations with implicit relaxation-zones

Robinson Perić, Vuko Vukčević, Moustafa Abdel-Maksoud, Hrvoje Jasak

- An analytical approach is presented for optimizing wave-generation and wave-damping when using implicit relaxation zones
- A computer program for optimizing the implicit relaxation zone based on the analytical approach was published as free software: <https://github.com/wave-absorbing-layers/relaxation-zones-for-free-surface-waves>
- The approach predicts the optimum values of the relaxation zone's case-dependent parameters and closely estimates the upper-limit for the corresponding wave-reflection coefficients
- Analytical predictions agree well with results from 2D- and 3D-flow simulations with strongly wave-reflecting bodies subjected to nonlinear free-surface waves

Optimizing wave-generation and wave-damping in 3D-flow simulations with implicit relaxation-zones

Robinson Perić^a, Vuko Vukčević^b, Moustafa Abdel-Maksoud^a and Hrvoje Jasak^{c,d}

^aHamburg University of Technology (TUHH), Institute for Fluid Dynamics and Ship Theory (M8), Hamburg, Germany

^bSimScale GmbH, Riddlerstrasse 31b, Munich, Germany

^cUniversity of Zagreb, Faculty of Mechanical Engineering and Naval Architecture, Ivana Lučića 5, Zagreb, Croatia

^dWikki Ltd, 459 Southbank House, SE1 7SJ, London, United Kingdom

ARTICLE INFO

Keywords:

Implicit relaxation-zones
free-surface waves
optimize wave-generation and wave-damping
reflection coefficient
case-dependent parameters

ABSTRACT

In finite-volume-based flow-simulations with free-surface waves, wave reflections at the domain boundaries can cause substantial errors in the results and must therefore be minimized. This can be achieved via ‘implicit relaxation zones’, but only if the relaxation zone’s case-dependent parameters are optimized. This work proposes an analytical approach for optimizing these parameters. The analytical predictions are compared against results from 2D-flow simulations for different water depths, flow solvers, and relaxation functions, and against results from 3D-flow simulations with strongly wave-reflecting bodies subjected to nonlinear free-surface waves. The present results demonstrate that the proposed approach satisfactorily predicts both the optimum parameter settings and the upper-limit for the corresponding reflection coefficients C_R . Simulation results for C_R were mostly below or equal to the analytical predictions, but never more than 3.4% larger. Therefore, the proposed approach can be recommended for engineering practice. Furthermore, it is shown that implicit relaxation zones can be considered as a special-case of forcing zones, a family of approaches which includes among others absorbing layers, damping zones and sponge layers. The commonalities and differences between these approaches are discussed, including to what extent the present findings are applicable to these other approaches and vice versa.

1. Introduction

In finite-volume-based flow simulations with free-surface waves, accurate wave-generation and wave-damping at the domain boundaries is important. Wave reflections at the boundaries of the computational domain can cause substantial errors in the results and must therefore be minimized (cf. Mani, 2012; Perić and Abdel-Maksoud, 2016; Vyzikas et al., 2017; Windt et al., 2019). This can be achieved by implementing *relaxation zones*, which gradually fade-out the simulated flow solution and blend-in a prescribed far-field wave solution near the domain boundaries.

Relaxation zones can be subdivided into *explicit* and *implicit relaxation zones*, which are fundamentally different:

Explicit relaxation zones (implemented e.g. in waves2Foam, cf. Jacobsen et al., 2012) modify the fields for volume fraction α and velocity \mathbf{u} by replacing computed values ϕ_{computed} by

$$\phi = (1 - b(\mathbf{x}))\phi_{\text{target}} + b(\mathbf{x})\phi_{\text{computed}}, \quad (1)$$

where $b(\mathbf{x})$ is a weighting function and ϕ_{target} is the target solution. This modification is performed in each time-step, e.g. prior to the solution of the pressure-velocity coupling (cf. Jacobsen et al., 2012). Among the most influential implementations of explicit relaxation zones are Mayer et al. (1998), Madsen et al. (2003), Engsig-Karup et al. (2006), Fuhrman et al. (2006), Jacobsen et al. (2012); further references and comparison to other wave-generation and wave-damping approaches can be found e.g. in Schmitt and Elsaesser (2015),

Windt et al., (2018, 2019) and Li et al., (2019). In contrast to implicit relaxation zones, it is not directly apparent to which source terms in the governing equations the ‘explicit’ manipulation of the flow field corresponds. Therefore, in this work the focus will be on implicit relaxation zones.


Implicit relaxation zones (implemented e.g. in Naval Hydro Pack, cf. Jasak et al.; 2015, Vukčević et al., 2016a, 2016b, 2017; Perić, 2019) introduce source terms in the governing equations to blend, say a general transport equation \mathcal{T} for transport quantity ϕ , over to a reference solution ϕ_{ref} via

$$(1 - b(\mathbf{x}))\mathcal{T} + \frac{b(\mathbf{x})}{\tau}\mathcal{R} = 0, \quad (2)$$

where $b(\mathbf{x})$ is a blending function such as Eq. (9), \mathcal{T} corresponds e.g. to the conservation equations for fluid momentum or volume fraction, and \mathcal{R} corresponds to $\int_V (\phi - \phi_{\text{ref}}) dV$.

The main problem with both explicit and implicit relaxation zones is that they provide satisfactory wave-generation and wave-damping *only if their case-dependent parameters are optimized*. However, how to optimize these case-dependent parameters before performing the flow-simulations has not been shown so far (cf. Miquel et al., 2018; Chen et al., 2019; Choi et al., 2020; Higuera, 2020). Thus at present, is it common practice to use either default or trial-and-error-based values for these parameters, which can lead to large errors in the results as will be demonstrated in this work.

Therefore, the first aim of this work is to present an analytical approach to optimize the case-dependent parameters of implicit relaxation zones, so that these can be optimized before performing the flow simulation.

 robinson.peric@tuhh.de (R. Perić)
ORCID(s):

Apart from relaxation zones, there exist various other approaches that generate and damp waves via domain-internal source terms. These approaches include ‘absorbing layers’ (e.g. Wei et al., 1999), ‘damping zones’ (e.g. Park et al., 1999, 2001), ‘dissipation zones’ (Park et al., 1993), ‘numerical beaches’ (e.g. Schmitt et al., 2019), ‘sponge layers’ (e.g. Israeli and Orszag, 1981; Larsen and Dancy, 1983; Choi and Yoon, 2009) or the ‘Euler overlay method’ (e.g. Kim et al., 2012). Recently, Perić (2019) showed that all these approaches can be formulated as special cases of a generic approach, called *forcing zones*. Forcing zones add source terms on the right-hand side of e.g. the conservation equations for velocity u_i and volume fraction α , to gradually force the flow towards a prescribed reference solution, $u_{i,\text{ref}}$ and α_{ref} , near the domain boundaries:

$$q_i = \int_V \rho \gamma b(\mathbf{x}) (u_{i,\text{ref}} - u_i) dV \quad , \quad (3)$$

$$q_\alpha = \int_V \gamma b(\mathbf{x}) (\alpha_{\text{ref}} - \alpha) dV \quad , \quad (4)$$

with volume V and fluid density ρ . The case-dependent parameters of forcing zones are the zone thickness x_d , the forcing strength γ , which regulates the source-term magnitude, and the blending function $b(\mathbf{x})$, which regulates how the source-term magnitude varies within the zone. The optimum values of these parameters can be determined analytically as shown by Perić and Abdel-Maksoud (2018). However, so far it is not known whether or to which extend the findings on the optimization of forcing zones are applicable to relaxation zones.

Therefore, the second aim of this work is to show how implicit relaxation zones are related to forcing zones, and to what extend findings obtained for forcing zones are applicable to implicit relaxation zones and vice versa.

Section 2 describes the governing equation for free-surface flows with implicit relaxation zones. Section 3 describes how to compute reflection coefficients, which are used to quantify how well waves are absorbed in the relaxation zone. Section 4 presents the analytical approach for optimizing the implicit relaxation zone. Sections 6 and 7 compare the analytical predictions against results from 2D- and 3D-flow simulations based on the setup from Sect. 5. Section 8 discusses the findings and the relation between forcing zones, explicit relaxation zones and implicit relaxation zones.

2. Governing equations with implicit relaxation zones

The conservation equations for momentum and volume fraction take the form

$$(1 - b(\mathbf{x})) \left[\frac{d}{dt} \int_V \rho u_i dV + \int_S \rho u_i (\mathbf{u} - \mathbf{u}_g) \cdot \mathbf{n} dS - \int_S (\tau_{ij} \mathbf{i}_j - p \mathbf{i}_i) \cdot \mathbf{n} dS - \int_V \rho \mathbf{g} \cdot \mathbf{i}_i dV \right]$$

$$+ \frac{b(\mathbf{x})}{\tau} \left[\int_V \rho (u_i - u_{i,\text{ref}}) dV \right] = 0 \quad , \quad (5)$$

$$(1 - b(\mathbf{x})) \left[\frac{d}{dt} \int_V \alpha dV + \int_S \alpha (\mathbf{u} - \mathbf{u}_g) \cdot \mathbf{n} dS \right] + \frac{b(\mathbf{x})}{\tau} \left[\int_V (\alpha - \alpha_{\text{ref}}) dV \right] = 0 \quad (6)$$

with reference velocities $u_{i,\text{ref}}$ and reference volume fraction α_{ref} . with volume V of control volume (CV) bounded by the closed surface S , fluid velocity $\mathbf{u} = (u_1, u_2, u_3)^T = (u, v, w)^T$, grid velocity \mathbf{u}_g , unit vector \mathbf{n} normal to S and pointing outwards, time t , pressure p , fluid density ρ , components τ_{ij} of the viscous stress tensor, unit vector \mathbf{i}_j in direction x_j , volume fraction α of water, reference velocities \mathbf{u}_{ref} and reference volume fraction α_{ref} .

Implicit relaxation zones have three case-dependent parameters: relaxation parameter τ , blending function $b(\mathbf{x})$, and relaxation zone thickness x_d .

The relaxation parameter τ has unit [s] and regulates the magnitude of the source term in such a way that a large value of τ implicates a small source term and vice versa¹.

The blending function $b(\mathbf{x})$ is bounded between 0 and 1. In this work, exponential-, cosine- and power-blending functions will be used

$$b(\mathbf{x}) = \left(\frac{e^{((x_d - \tilde{x})/x_d)^n} - 1}{e^n - 1} \right) \quad , \quad (7)$$

$$b(\mathbf{x}) = \left[\cos^2 \left(\frac{\pi}{2} + \frac{\pi}{2} \left(\frac{x_d - \tilde{x}}{x_d} \right) \right) \right]^n \quad , \quad (8)$$

$$b(\mathbf{x}) = \left(\frac{x_d - \tilde{x}}{x_d} \right)^n \quad , \quad (9)$$

where \tilde{x} is the shortest distance to the closest domain boundary to which a relaxation zone of thickness x_d is attached (confer Fig. 1), and n regulates the shape of the blending function. Outside the relaxation zone holds $b(\mathbf{x}) = 0$.

3. Determining reflection coefficient C_R for implicit relaxation zones

For regular, long-crested waves entering a relaxation zone with normal incidence, the reflection coefficient is $C_R = H_R/H$ in terms of the wave heights H_R and H of the reflected and the generated wave, respectively.

Following Ursell et al. (1960), C_R can be computed via

$$C_R = (H_{\text{max}} - H_{\text{min}}) / (H_{\text{max}} + H_{\text{min}}) \quad , \quad (10)$$

¹Note that in some publications τ has been considered a numerical-stability parameter and has therefore occasionally been omitted from Eq. (2). However, the present work demonstrates the physical meaning of τ and also that its optimum value does not necessarily coincide with the value which gives the most favorable matrix conditioning.

where H_{\max} and H_{\min} are the overall largest and smallest wave heights that occur, e.g. in this work, during the last simulated wave period over a distance of ca. one wavelength outside but adjacent to the relaxation zone. This approach has a comparatively small background noise of ca. 1% (cf. Perić and Abdel-Maksoud, 2018; Perić, 2019), i.e. reflection coefficients $C_R \lesssim 0.01$ cannot be detected.

However, before the output of Eq. (10) qualifies as reflection coefficient, additional requirements must be fulfilled: The domain size and simulation duration must be chosen so that wave reflections have fully developed in the evaluation interval, while possible wave re-reflections (e.g. at the inlet boundary) have not yet traveled back into the evaluation interval. Further, it must hold $0 \leq C_R \leq 1$, with $C_R = 0$ for no wave reflection and $C_R = 1$ for perfect wave reflection. Therefore, the boundary conditions must be chosen so that $C_R = 1$ is obtained if the source terms are set to zero, which is discussed in more detail in Sect. 6.4. Unless mentioned otherwise, these requirements are fulfilled in the present work.

4. Analytical approach for optimizing the case-dependent parameters in implicit relaxation zones

This section proposes an analytical approach to predict the optimum values for the case-dependent parameters in implicit relaxation zones. For this, the analytical solution from Perić and Abdel-Maksoud (2018) is extended to implicit relaxation zones, by reformulating them into (mathematically) ‘equivalent forcing zones’.

The implicit relaxation zone can be interpreted as a forcing zone (cf. Perić, 2019), when Eqs. (5) and (6) are multiplied by the factor $1/(1 - b(\mathbf{x}))$, which gives

$$\begin{aligned} \frac{d}{dt} \int_V \rho u_i dV + \int_S \rho u_i (\mathbf{u} - \mathbf{u}_g) \cdot \mathbf{n} dS = \\ \int_S (\tau_{ij} \mathbf{i}_j - p \mathbf{i}_i) \cdot \mathbf{n} dS + \int_V \rho \mathbf{g} \cdot \mathbf{i}_i dV + \int_V \rho q_i dV \quad , \end{aligned} \quad (11)$$

$$\frac{d}{dt} \int_V \alpha dV + \int_S \alpha (\mathbf{u} - \mathbf{u}_g) \cdot \mathbf{n} dS = \int_V q_\alpha dV \quad , \quad (12)$$

with forcing source-terms

$$q_i = \int_V \rho \gamma b(\mathbf{x}) (u_{i,\text{ref}} - u_i) dV \quad , \quad (13)$$

$$q_\alpha = \int_V \gamma b(\mathbf{x}) (\alpha_{\text{ref}} - \alpha) dV \quad , \quad (14)$$

where the forcing strength γ is set to

$$\gamma = \left(\frac{\bar{E}_{\text{kin},x} + \bar{E}_{\text{kin},y} + \bar{E}_{\text{kin},z} + \bar{E}_{\text{pot}}}{\bar{E}_{\text{kin},x}} \right) \frac{1}{\tau(1 - b(\mathbf{x}))} \quad ,$$

with control volume V , fluid density ρ , location \mathbf{x} , kinetic \bar{E}_{kin,x_i} and potential \bar{E}_{pot} wave energy components², relaxation parameter τ and blending function $b(\mathbf{x})$.

For given blending function $b(\mathbf{x})$ and zone thickness x_d , the optimum value of γ in Eq. (15) can be computed analytically as given in Perić and Abdel-Maksoud (2018). Therefore, the optimum value of τ can be obtained by rearranging Eq. (15). A simple computer program to optimize implicit relaxation zones has been published as free software: <https://github.com/wave-absorbing-layers/relaxation-zones-for-free-surface>

The derivation of the analytical solution for Eqs. (11–15) in Perić and Abdel-Maksoud (2018) neglects some flow phenomena of minor importance, such as that reflected wave components due to source terms in different governing equations can have different phases and may partially cancel destructively. Thus, actual reflection coefficients can be lower than predicted via Eq. (15). Apart from this, the following can be expected from literature (Perić, 2019; Perić and Abdel-Maksoud, 2016, 2018, 2020):

The optimum value of relaxation parameter τ will be closely predicted. The predictions for reflection coefficient C_R can be taken as estimates for the upper-limit of the actual reflection coefficients in the simulations. The implicit relaxation zones behave discretization-independent for practical discretizations (i.e. more than ca. 30 cells per wavelength).

For irregular waves, the overall reflection coefficient C_R can be estimated based on the reflection coefficients of each wave component.

For nonlinear waves, the analytical approach can be applied without modification, because, for optimized parameters, partial wave-reflection occurs throughout the relaxation zone with small amplitudes (i.e. nearly linear waves), which can interfere destructively. This ability to ‘linearize’ nonlinear waves makes relaxation zones applicable to highly nonlinear, complex flows, because they produce basically the same amount of reflection regardless of the wave’s nonlinearity. This is their main advantage compared to boundary-based approaches such as absorbing boundary conditions, where a complex nonlinear solution must be prescribed at the domain boundary and reflection coefficients can increase unpredictably with flow nonlinearity.

For oblique wave incidence, the analytical approach above can be extended to provide the reflection coefficient as a function of the wave-incidence angle. Results from 3D-flow simulations with strongly reflecting bodies in waves suggest that the analytical approach for 2D-wave propagation as out-

²Note that \bar{E}_{kin,x_i} and \bar{E}_{pot} are not evaluated from the simulation results, but only their ratios are important, which can be taken from wave theory. The reason for the appearance of these terms is that in shallow water, the vertical kinetic energy component vanishes, and consequently the influence of the source terms in the equation for the vertical fluid momentum vanishes. Therefore, to obtain a forcing or relaxation with the same source term magnitude in shallow water as in deep water, the magnitude of the source terms must be increased in shallow water. This effect is comparatively small; it can change the optimum values for γ or τ by a factor of 2 at most. Therefore, the factor containing the wave energy components in Eq. (15) can be computed from linear wave theory.

Table 1

Wave parameters for the different simulation setups: wave height H , wave period T , wavelength λ , water depth h , wave steepness H/λ in terms of maximum wave steepness $(H/\lambda)_{\max}$

	H	T	λ	$\frac{H/\lambda}{(H/\lambda)_{\max}}$
2D, deep water	0.16 m	1.6 s	4 m	28.6%
2D, shallow water	0.009 m	2.893 s	4 m	22.5%
3D, deep water	0.4 m	1.6 s	4.3 m	65.5%

lined above typically suffices to optimize the relaxation zone's parameters.

5. Simulation setup

For the 2D-simulations in Sects. 6.1 to 6.5, the solution domain is box-shaped as seen in Fig. 1. The origin of the coordinate system lies at the calm free-surface level, with z pointing upwards and x pointing in wave propagation direction. The domain dimensions are $0 \text{ m} \leq x \leq 24 \text{ m}$, $-2 \text{ m} \leq z \leq 0.24 \text{ m}$ for the simulations with deep water conditions (water depth $h \approx 0.5\lambda$) and $0 \text{ m} \leq x \leq 24 \text{ m}$, $-0.2 \text{ m} \leq z \leq 0.01 \text{ m}$ for the simulations with shallow water conditions ($h \approx 0.05\lambda$). The simulations are quasi-2D, i.e. there is only one layer of cells in y -direction and the y -normal boundaries set to symmetry planes.

Waves are generated by prescribing volume fraction α and velocities \mathbf{u} according to Rienecker and Fenton's (1981) stream function wave theory (64th order) at the velocity inlet $x = 0$. Table 1 gives the wave parameters. The waves travel in positive x -direction towards an implicit relaxation zone attached to the pressure outlet boundary at $x = 24 \text{ m}$. At the outlet, pressure and volume fraction are prescribed according to the calm free-surface solution.

The governing equations are Eqs. (5) to (6). In the implicit relaxation zone, velocity \mathbf{u} and volume fraction α are blended towards the analytical reference solution, \mathbf{u}_{ref} and α_{ref} , to reduce undesired wave reflections. The relaxation zone's parameters are optimized according to the analytical approach presented in Sect. 4. Simulations are performed for different values of zone thickness x_d , different blending functions $b(\mathbf{x})$, and different reference solutions. The bottom boundary has a slip-wall boundary condition and at the top boundary atmospheric pressure is prescribed.

The simulations in this work are performed using foam-extend version 4.1, an open-source fork of the flow-solver OpenFOAM (Weller et al., 1998), combined with the commercial software Naval Hydro Pack. The governing equations are Eqs. (5) to (6), so no turbulence modeling is used. All approximations are of second order. The solvers are conjugate gradient with Incomplete Cholesky preconditioner for pressures and bi-conjugate gradient with ILU0 preconditioner for volume fraction and velocities. The PIMPLE scheme is used with two pressure-correction steps per each of the two nonlinear iterations per time step. No under-relaxation is used. In all simulations, the Courant number $C = |\mathbf{u}|\Delta t/\Delta x$ remains well below 0.4. Further information on the dis-

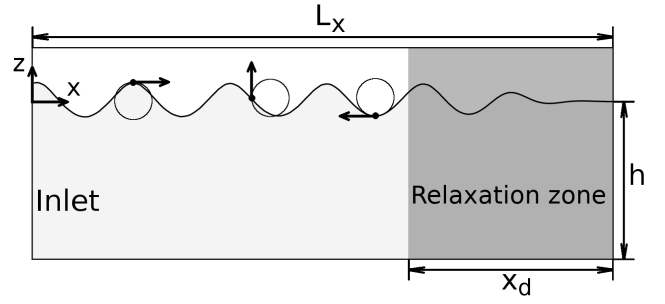


Figure 1: Solution domain filled with air (white) and water (light gray, water depth h), velocity inlet at $x = 0$ and implicit relaxation zone (shaded dark gray) with thickness x_d ; three fluid particles (black dots) are sketched with their particle paths (circles) and velocity vectors (arrows)

cretization of and solvers for the governing equations can be found in Ferziger and Perić (2020) and the flow solver manuals.

Figure 2 shows the rectilinear grid with local mesh refinement. The free surface remains at all times within the zone with the finest mesh, with 25 (coarse grid), 35 (medium grid), or 50 (fine grid) cells per wavelength λ , and 5 (coarse grid), 7 (medium grid), or 10 (fine grid) cells per wave height H . The grid consists of 12 000 (coarse grid), 27 000 (medium grid), or 48 000 (fine grid) cells. The time-step is $0.01 \text{ s} = T/160$ (coarse grid), $0.0071 \text{ s} = T/226$ (medium grid), or $0.005 \text{ s} = T/320$ (fine grid). The reflection coefficient C_R is calculated as given in Sect. 3.

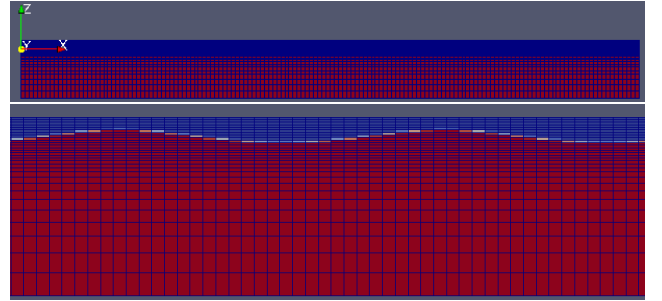


Figure 2: Mesh for 2D-flow simulations with coarse grid; far view (top) and close-up (bottom); the color denotes the volume fraction (red: water, blue: air)

In Sect. 6.3, selected simulations were repeated with the commercial flow solver STAR-CCM+ version 10.6 by Siemens, using the grid and simulation setup from Perić and Abdel-Maksoud (2018), except that the forcing zones in STAR-CCM+ were optimized via Eqs. (13) to (15) in such a way that they mimic the behavior of the implicit relaxation zones from the Naval Hydro Pack.

For the 3D-simulations in Sect. 7, the setup is identical to the deep-water 2D simulations, with the following exceptions. The domain has dimensions $0 \text{ m} \leq x \leq 10 \text{ m}$, $0 \text{ m} \leq y \leq 10 \text{ m}$, $-5 \text{ m} \leq z \leq 5 \text{ m}$, so the water depth is

$h = 5$ m as seen in Fig. 3. In the center of the domain, a semi-submerged pontoon with dimensions $1 \text{ m} \times 1 \text{ m} \times 1 \text{ m}$ is held in fixed position as seen in Fig. 15. It has a draft of $D = 0.5$ m and slip wall boundary conditions. The wave parameters are given in Table 1.

The relaxation zone thickness is $x_d = 3 \text{ m} \approx 0.7\lambda$ and power blending according to Eq. (9) with exponent $n = 0.46$ is used. Simulations are performed for different relaxation parameters $0.001 \text{ s} \leq \tau \leq 1000 \text{ s}$. This setup is expected to be close to the minimum domain size for the simulation of such a strongly wave-reflecting body.

The free surface is discretized by 12.9 (coarse grid), 25.8 (medium grid), or 38.7 (fine grid) cells per wavelength λ and 2 (coarse grid), 4 (medium grid), or 6 (fine grid) cells per wave height H as shown in Fig. 3. Per wave period 160 (coarse grid), 225 (medium grid), or 320 (fine grid) time steps are used.

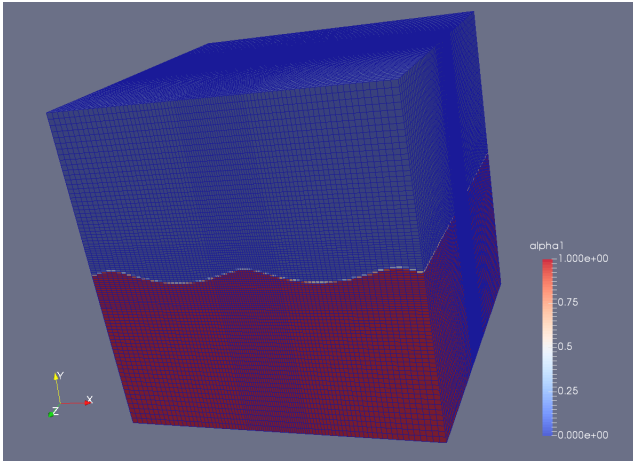


Figure 3: Fine mesh for 3D-flow simulations with initialized volume fraction

6. Results from 2D-flow simulations

This section compares the analytical predictions from Sect. 4 against results from 2D-flow simulations based on the 2D-setup from Sect. 5.

6.1. Discretization dependence study for wave damping via implicit relaxation zones in deep water

This section investigates wave damping via implicit relaxation zones in deep water. To damp the waves, the reference solution in Eqs. (5) and (6) is set to the hydrostatic solution for the calm free-surface. Exponential blending via Eq. (7) with coefficient $n = 3.5$ is used, which is the default setting in the Naval Hydro Pack. Simulations are performed for different values of zone thickness x_d and relaxation parameter τ .

Figure 4 demonstrates for different zone thicknesses x_d that the analytical approach proposed in Sect. 4 predicts the

optimum value of relaxation parameter τ closely. As expected from the discussion in Sect. 4, the analytical predictions additionally provide a satisfactory estimate of the upper-bound for reflection coefficient C_R .

Note that the lower plot in Figs. 4, 6 and 9 shows the same data as the upper plot but with a logarithmic vertical axis, to better visualize the results for small values of reflection coefficient C_R . Furthermore, note that due to the slight background-noise in the scheme for determining C_R , reflection coefficients below ca. 0.01 cannot be detected reliably. Finally, note that the curves in each plot hold only for the given wave period T ; when the wave period changes, the curves shift sideways.

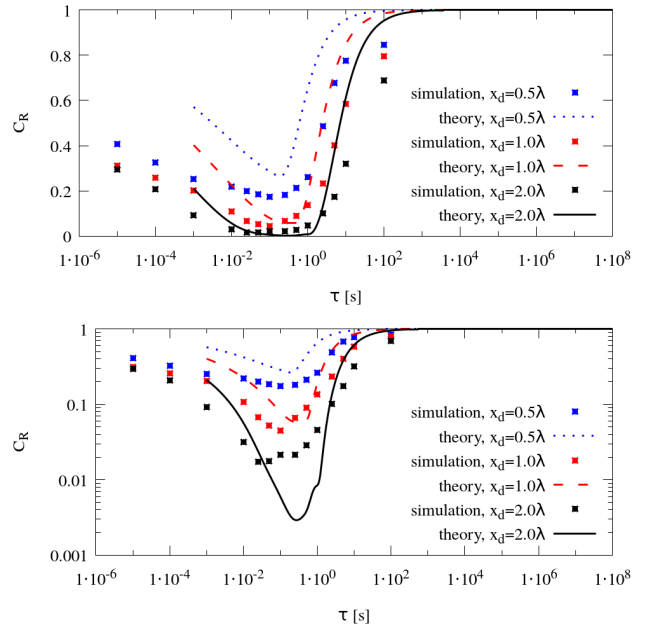


Figure 4: Analytical predictions ('theory') and simulation results ('simulation') for reflection coefficient C_R as a function of relaxation parameter τ , for deep-water waves with period $T = 1.6$ s; for exponential blending via Eq. (7) with exponent $n = 3.5$, coarse discretization and different values of relaxation zone thickness x_d ; for all simulation results $C_{R,\text{sim}}$ and corresponding analytical predictions $C_{R,\text{theory}}$ holds $C_{R,\text{sim}} - C_{R,\text{theory}} < 3.8\%$; for the forcing strength $\tau \leq \tau_{\text{opt,theory}}$ closest to the theoretical optimum value $\tau_{\text{opt,theory}}$ holds $C_{R,\text{sim}} - C_{R,\text{theory}} < 1.9\%$

Figure 5 demonstrates that, for practical discretizations (i.e. 25 or more cells per wavelength λ), implicit relaxation zones behave basically discretization-independent. The slight background-noise in the scheme for determining reflection coefficient C_R was attributed to the interface-sharpening scheme (cf. Larsen et al., 2019; Berndt et al., 2021).

6.2. Wave damping via implicit relaxation zones in shallow water

This section investigates wave damping via implicit relaxation zones in shallow water. The derivation in Sect. 4 holds for all water depths, and Fig. 6 confirms that its predictions are of satisfactory accuracy also in shallow water.

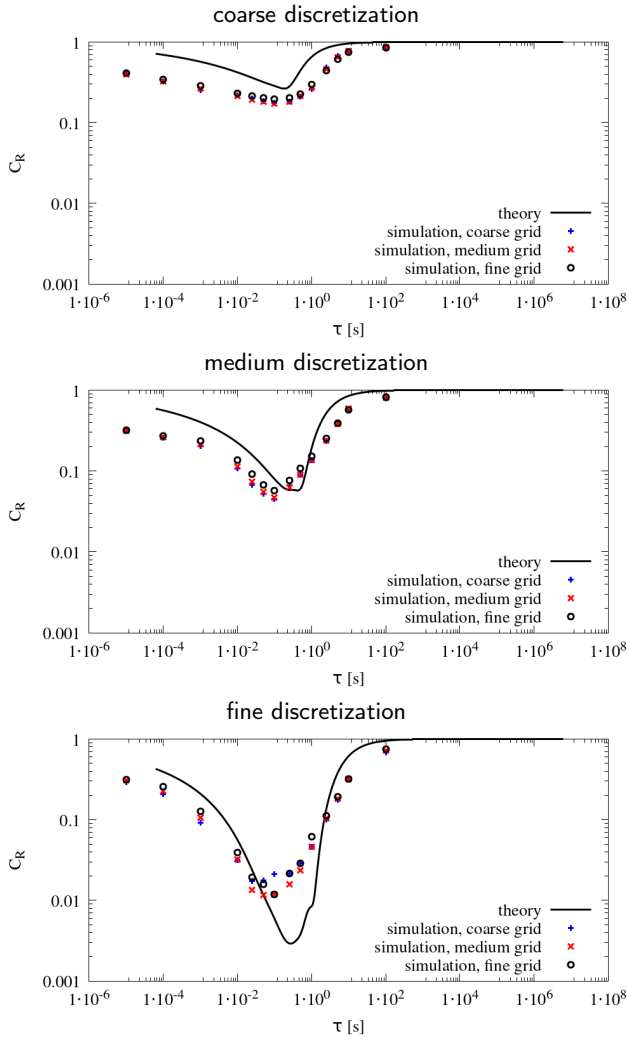


Figure 5: As Fig. 4, except for coarse, medium, and fine discretization from Sect. 5; as theory suggests, results can be considered discretization-independent for practical discretizations; for all simulation results $C_{R,\text{sim}}$ and corresponding analytical predictions $C_{R,\text{theory}}$ holds $C_{R,\text{sim}} - C_{R,\text{theory}} < 5.3\%$; for the relaxation parameter $\tau \leq \tau_{\text{opt,theory}}$ closest to the theoretical optimum value $\tau_{\text{opt,theory}}$ holds $C_{R,\text{sim}} - C_{R,\text{theory}} < 1.9\%$

Compared to the deep-water case from Sect. 6.1, the simulation results for reflection coefficient C_R are lower for smaller-than-optimum values of relaxation parameter τ , but show no substantial qualitative difference otherwise. This was expected, because Perić (2019) showed that in shallow water (where the horizontal components of the average kinetic wave energy are much larger than the vertical component), stronger-than-optimum forcing of volume fraction α reflects waves with a phase shift of 180deg compared to forcing of horizontal velocity u , so that combined α - and u -forcing produces destructive interference and thus lower reflection coefficients C_R than in deep water (where the horizontal and vertical components of the average kinetic energy have the same magnitude).

Recently, Carmigniani and Violeau (2018) used forcing

zones for horizontal and vertical velocities to damp regular waves in finite-difference-based flow simulations for linearized Navier-Stokes-equations; they observed a decrease in the optimum value of the source term strength for decreasing water depth. In contrast, the present results show no significant dependence of the optimum value of relaxation parameter τ on the water depth.

However, one should point out that, in Figs. 4 to 10, the optimum τ -value from the simulation results is sometimes slightly larger or smaller than predicted analytically. The relaxation parameter $\tau_{\text{opt,sim}}$ for the simulation result with the lowest reflection coefficient C_R took values within $\tau_{\text{opt,sim}} \in [\frac{1}{12}\tau_{\text{opt,theory}}, 2\tau_{\text{opt,theory}}]$, where $\tau_{\text{opt,theory}}$ denotes the theoretically predicted optimum τ -value. Since there did not seem to be a clear trend in these deviations and since they were comparatively small, this detail seems to be of minor importance for engineering practice.

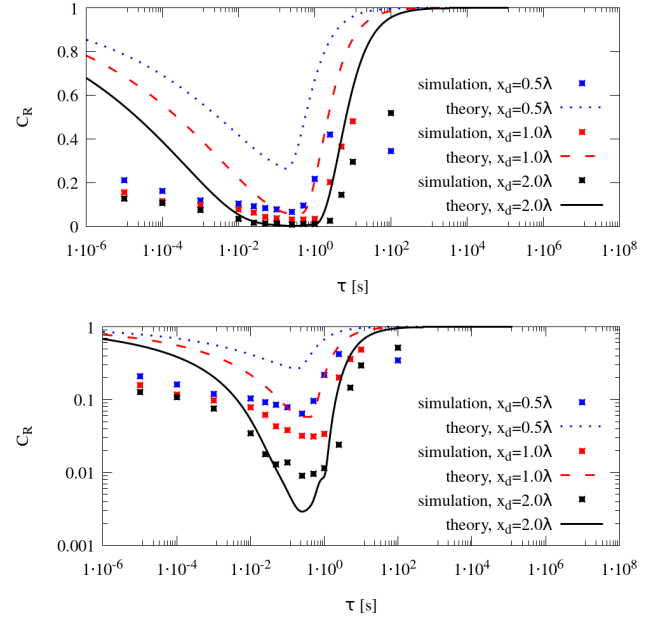


Figure 6: As Fig. 4, except for shallow-water waves with period $T = 2.893$ s; for all simulation results $C_{R,\text{sim}}$ and corresponding analytical predictions $C_{R,\text{theory}}$ holds $C_{R,\text{sim}} - C_{R,\text{theory}} < 0.8\%$; for the forcing strength $\tau \leq \tau_{\text{opt,theory}}$ closest to the theoretical optimum value $\tau_{\text{opt,theory}}$ holds $C_{R,\text{sim}} - C_{R,\text{theory}} < 0.5\%$

6.3. Comparison between implicit relaxation zones and equivalent forcing zones in a different flow solver

This section aims to validate the finding from Sect. 4, that implicit relaxation zones can be interpreted as a special-case of forcing zones. For this, flow simulations with wave damping via implicit relaxation zones are performed for different blending functions $b(\mathbf{x})$ with a similar setup as in Sect. 6.1. Then, the flow simulations are repeated using a different flow solver, Siemens STAR-CCM+, with an ‘equivalent forcing zone’ instead of the implicit relaxation zone, and the

results are compared.

The ‘equivalent forcing zone’ is constructed as follows: In STAR-CCM+, forcing zones according to Eqs. (11) and (12) are available. To ‘mimick’ the behavior of an implicit relaxation zone, the forcing strength γ is selected as given in Eq. (15).

Note that ‘mimicking’ relaxation zones via forcing zones is performed here only to demonstrate the close relationship between both approaches. In practice, such ‘mimicking’ is not recommended: Even if it results should theoretically be the same, ‘mimicking’ can impair the numerical stability. For example, in the ‘equivalent forcing zone’ outlined above holds near the domain boundary $b(\mathbf{x}) \rightarrow 1$, so that the source term magnitude would approach infinity. Thus stability problems must be expected for the ‘equivalent forcing zone’ when relaxation parameter $\tau \rightarrow 0$ and when the cell sizes close to the domain boundary are small. The STAR-CCM+ simulations indeed blew up for small τ -values, which is the reason for the missing data points ($\tau \leq 10^{-2}$ s) in Figs. 7 and 8.

No stability issues occur when forcing zones (Eqs. (11) to (12)) or implicit relaxation zones (Eqs. (5) and (6)) are used in the way they were intended, as the results in the other sections or in literature (e.g. Perić, 2019; Perić and Abdel-Maksoud, 2018, 2020) demonstrate. Further, comparing the present results to the ones from literature indicates that forcing zones and implicit relaxation zones both work equally satisfactory when correctly set up.

Figures 7 and 8 show that the results of the two different codes agree well. Thus one can confidently expect both the present results and the analytical approach from Sect. 4 to be applicable to other computational-fluid-dynamics solvers as well.

6.4. Relaxation towards far-field wave vs. relaxation towards calm-water solution

This section investigates the influence of the choice of reference solution for implicit relaxation zones. In practice, the reference solution is often the far-field wave solution. Therefore, the simulations from Sect. 6.1 were repeated with reference solution \mathbf{u}_{ref} and α_{ref} set to the stream function solution for the far-field wave.

Figure 9 shows that, although Sects. 6.1 and 6.4 use substantially different reference solutions, again the optimum value for relaxation parameter τ is well predicted.

However, compared to Fig. 4, the values for reflection coefficient C_R in Fig. 9 are substantially lower, which becomes more pronounced on the fine discretization. The reason for this is that the C_R -values in Fig. 9 do not qualify as reflection coefficients (cf. definition in Sect. 3), because the simulation setup does not yield $C_R = 1$ if the relaxation zone is switched off: There is no flow disturbing body within the domain, so differences between the computed and reference solution are mainly due to discretization and iteration errors, which vanish on the finer grids; the smaller the differences between computed and reference solution are, the smaller will be wave reflections at the outlet boundary, where

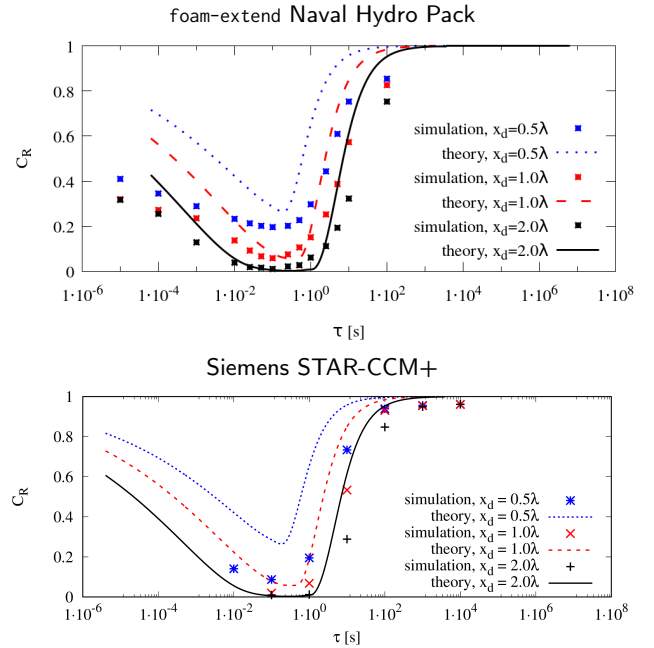


Figure 7: Analytical predictions (‘theory’) and simulation results (‘simulation’) from two different CFD codes for reflection coefficient C_R as a function of relaxation parameter τ , for deep-water waves with period $T = 1.6$ s; for fine discretization, exponential blending via Eq. (7) with exponent $n = 3.5$ and different values of zone thickness x_d ; for implicit relaxation zone (top) and its ‘equivalent forcing zone’ (bottom)

the reference solution is prescribed. In practice, the wave entering the relaxation zone usually does not correspond to the far-field wave, because it will be modified by wave reflecting bodies or discretization and iteration errors within the domain. Thus, for the general case of relaxation towards the far-field wave, one should rather expect reflection coefficients C_R as in Fig. 4.

6.5. Influence of choice of blending function $b(\mathbf{x})$

This section investigates how changing the blending function $b(\mathbf{x})$ can affect the behavior of implicit relaxation zones. For this, the simulations from Sect. 6.1 were repeated using different blending functions.

Figure 10 shows results for power blending according to Eq. (9) with different values of relaxation parameter τ , zone thickness x_d , and coefficient n . The results demonstrate that, depending on the choice of these parameters, the optimum value for relaxation parameter τ can vary by three orders of magnitude, which underlines the importance of optimizing the relaxation zone’s parameters. As before, the optimum value for τ is well predicted by the analytical approach.

For $\tau \rightarrow \infty$, the relaxation source terms vanish to zero, so one would expect that the solution behaves as if there were no relaxation zone; this would result in a standing wave (i.e. $C_R \approx 1$), since the outlet boundary is nearly perfectly reflecting. Instead, for large τ -values the reflection coefficients C_R

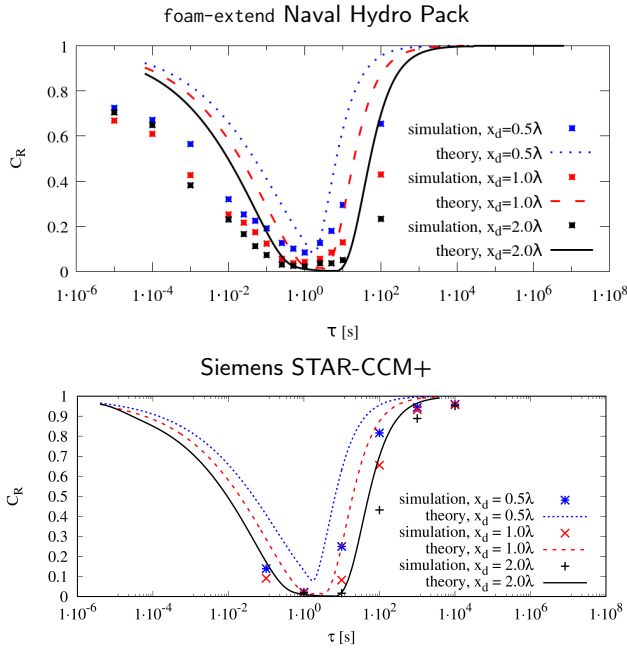


Figure 8: As Fig. 7, except that linear blending according to Eq. (9) with $n = 1$ was used; for all simulation results $C_{R,\text{sim}}$ and corresponding analytical predictions $C_{R,\text{theory}}$ holds $C_{R,\text{sim}} - C_{R,\text{theory}} < 3.9\%$; for the forcing strength $\tau \leq \tau_{\text{opt,theory}}$ closest to the theoretical optimum value $\tau_{\text{opt,theory}}$ holds $C_{R,\text{sim}} - C_{R,\text{theory}} < 3.4\%$

were significantly lower than 1, with lower values for smaller values of n . It is possible that this is due to the term $(1 - b(\mathbf{x}))$ on the left-hand side of the governing equations: If there is no reference solution to blend over to, then the blending out of the flow solution may behave like a damping. Note though that such large τ -values are not of practical interest, because they cannot be used for combined generation and damping of waves as is illustrated in Sect. 7 in Figs. 13 and 15.

Not only do the optimum values for τ and the curves for reflection coefficient $C_R(\tau)$ change as a function of the blending function $b(\mathbf{x})$ (cf. Fig. 10), but also the optimum choice of blending function (or here: its coefficient n) depends on the zone thickness x_d as Figs. 11 and 12 demonstrate. The optimum choice of n would correspond to the setting that provides both the lowest reflection coefficient C_R for optimized τ and the broadest range of adjacent τ -values, for which the reflection coefficient C_R will be below a given threshold; the broader this range, the less sensitive will the reflection behavior of the relaxation zone be to changes of the wave period. Thus, irregular waves with a broad-banded wave energy spectrum can require a different (possibly larger) n -value than monochromatic waves.

For the investigated blending functions in Figs. 11 and 12, the larger the relaxation zone thickness x_d becomes, the larger becomes the optimum value for n . For practical choices of x_d , the tendency appears to be that n should be < 1 for $x_d \lesssim 1.0\lambda$ and that n should be > 1 for $x_d \gtrsim 1.5\lambda$.

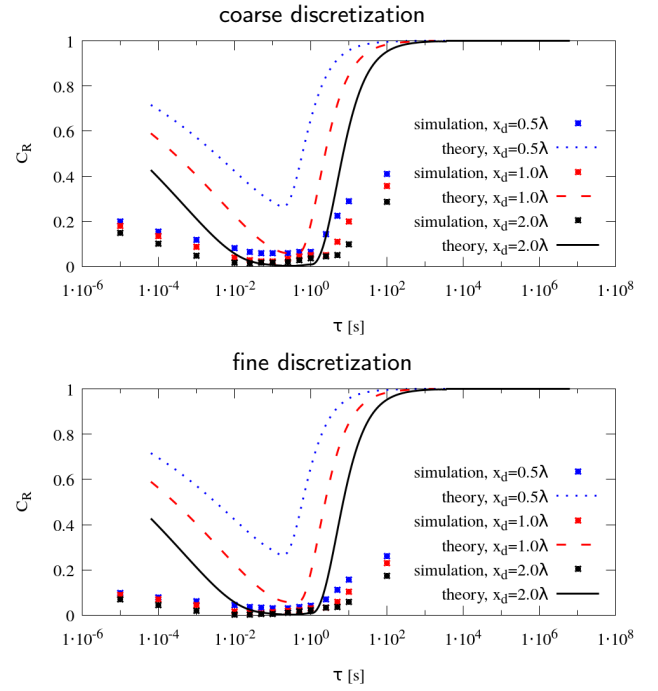


Figure 9: As Fig. 4, except for relaxation towards the far-field wave; for all simulation results $C_{R,\text{sim}}$ and corresponding analytical predictions $C_{R,\text{theory}}$ holds $C_{R,\text{sim}} - C_{R,\text{theory}} < 2.9\%$; for the forcing strength $\tau \leq \tau_{\text{opt,theory}}$ closest to the theoretical optimum value $\tau_{\text{opt,theory}}$ holds $C_{R,\text{sim}} - C_{R,\text{theory}} < 1.6\%$

7. Results from 3D-flow simulations

To investigate the validity of the present findings for practical 3D-flow simulations, the flow around a strongly reflecting semi-submerged pontoon subjected to steep deep-water waves is simulated with the setup from Sect. 5. The solution domain was selected intentionally small, with implicit relaxation zones attached to all vertical domain boundaries with a zone thickness of only $x_d \approx 0.7\lambda$. With respect to the tuning for the optimum blending function from Sect. 6.5, a power blending according to Eq. (9) with coefficient $n = 0.46$ was used. According to the analytical prediction, a relaxation parameter of $\tau = 2.5$ s should provide a satisfactory reduction of undesired wave reflections ($C_R \lesssim 5\%$), whereas τ -values larger or smaller by a factor of $10^{\pm 1}$ should produce significant reflections.

If reflections are satisfactorily reduced, then a periodic solution is expected to occur after several wave periods, and long-time simulations should be possible without the accumulation of errors due to undesired wave reflections. Figure 13 shows that indeed such periodic results are obtained for the optimum setting.

Figure 14 shows that the correct tuning of the relaxation zone enables a periodic solution for simulations over arbitrarily long simulation times. That the analytical solution from Eqs. (11)-(15) applies with good approximation to the 3D-case as well has been shown both analytically and via 3D-flow simulations for a comparable case in Perić and Abdel-

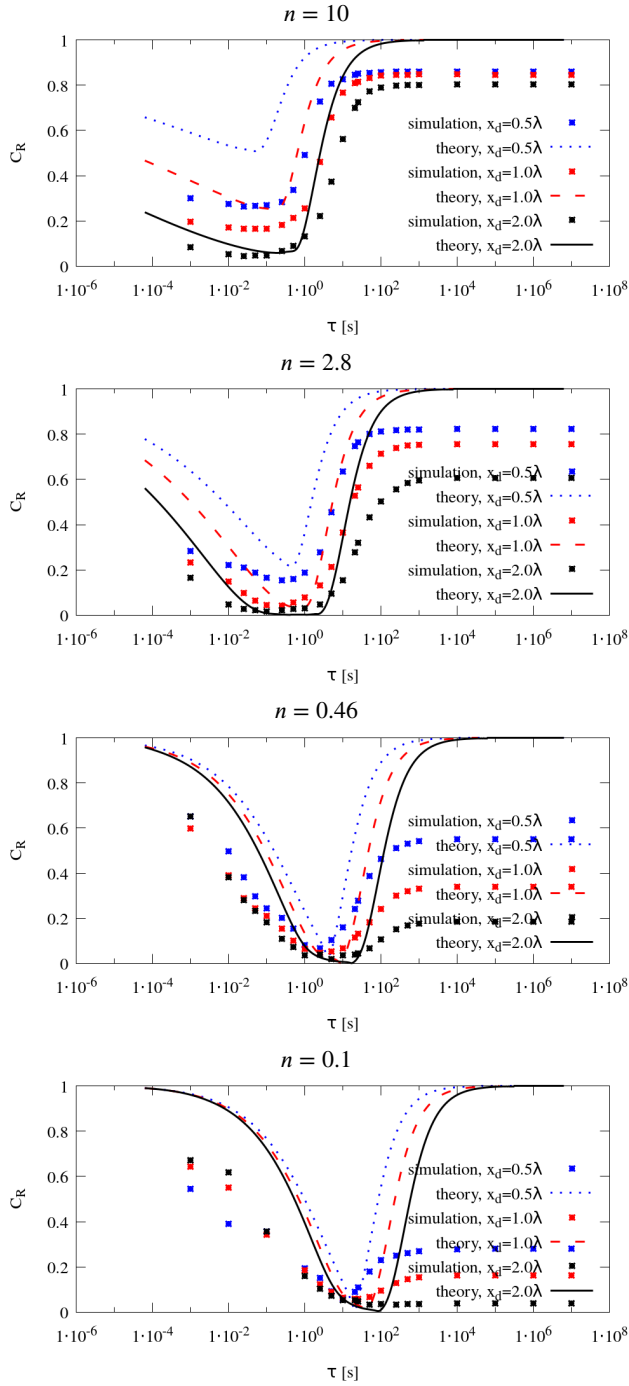


Figure 10: As Fig. 4, except for power blending via Eq. (9) with different values for exponent n ; the analytical approach ('theory') predicts the shift in optimum value for τ when changing exponent n ; for all simulation results $C_{R,\text{sim}}$ and corresponding analytical predictions $C_{R,\text{theory}}$ holds $C_{R,\text{sim}} - C_{R,\text{theory}} < 8.4\%$ ($n = 0.1$), $< 4.7\%$ ($n = 0.46$), $< 4.2\%$ ($n = 2.8$), and $< 2.3\%$ ($n = 10$); for the forcing strength $\tau \leq \tau_{\text{opt,theory}}$ closest to the theoretical optimum value $\tau_{\text{opt,theory}}$ holds $C_{R,\text{sim}} - C_{R,\text{theory}} < 2.7\%$ ($n = 0.1$), $< 3\%$ ($n = 0.46$), $< 2.0\%$ ($n = 2.8$), and $< -1.5\%$ ($n = 10$)

Maksoud (2020,2021) and is not repeated here.

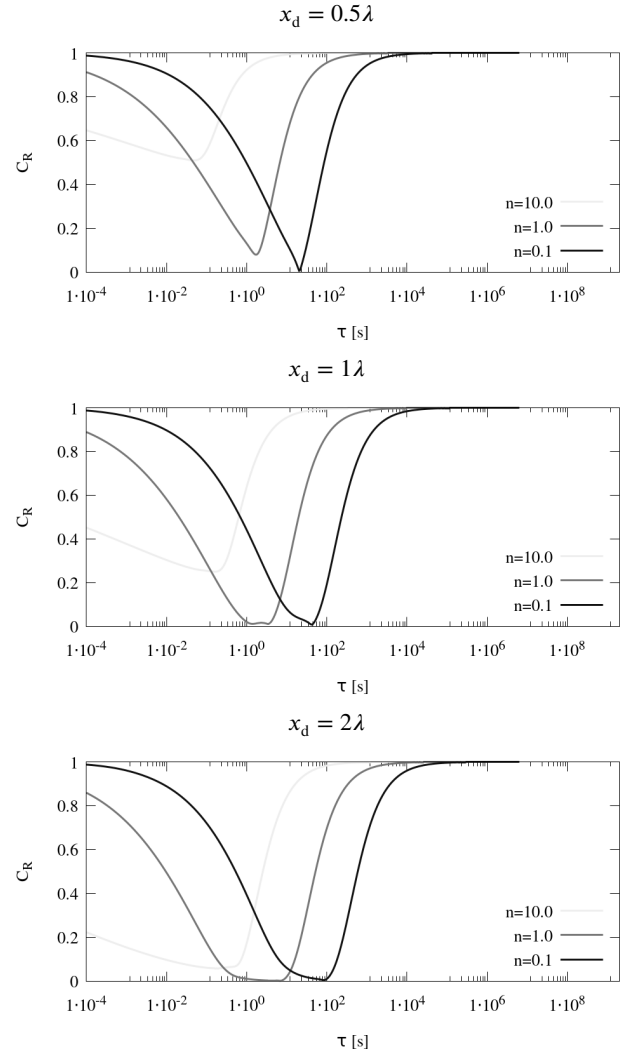


Figure 11: Analytical predictions ('theory') for reflection coefficient C_R as a function of relaxation parameter τ for deep-water waves with period $T = 1.6$ s; for power blending according to Eq. (9) with different values for exponent n

As shown in Fig. 15, too-strong relaxation (corresponding to smaller-than-optimum τ -values) produces wave reflections mainly at the entrance to the relaxation zone, resulting in a change of amplitude as well as aperiodicity of the forces on the pontoon (cf. Fig. 13, upper plot). Too-weak relaxation (corresponding to larger-than-optimum τ -values) damps not only the undesired wave reflections, but also the incident wave, so that the far-field wave is not sustained anymore, resulting in too-low forces on the pontoon (cf. Fig. 13, bottom plot).

Figures 16 and 17 show that the difference between medium and fine grid is comparatively small, but for the coarse grid the force amplitudes are ca. 10% lower. For the present purposes, all grids were considered suitable to demonstrate the benefits of tuning relaxation zones to the wave parameters.

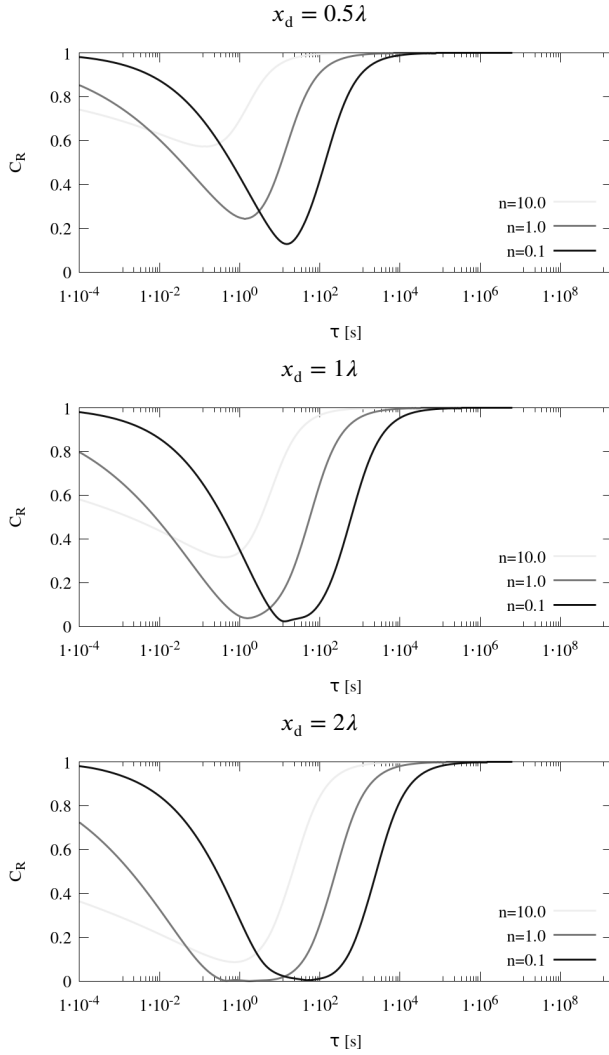


Figure 12: As Fig. 11, except for \cos^{2n} -blending according to Eq. (8) with different values for exponent n ; the optimum exponent n increases with increasing zone thickness x_d

8. Discussion

The results from Sects. 6 and 7 show that the analytical approach presented in Sect. 4 is suitable for optimizing the case-dependent parameters of implicit relaxation zones, both for 2D- and complex 3D-flow simulations with nonlinear free-surface waves. When the implicit relaxation zones were optimized according to the analytical approach, the simulation results for reflection coefficient C_R were mostly lower or equal their analytical predictions, but never more than 3.4% larger.

The analytical approach from Sect. 4 closely predicted the optimum relaxation-zone parameters. For all simulation results, the optimum value for relaxation parameter τ was within $[\frac{1}{12}\tau_{\text{opt,theory}}, 2\tau_{\text{opt,theory}}]$ in terms of the analytically predicted optimum $\tau_{\text{opt,theory}}$.

It was found that simulation results for reflection coefficient C_R can be lower than predicted analytically, which

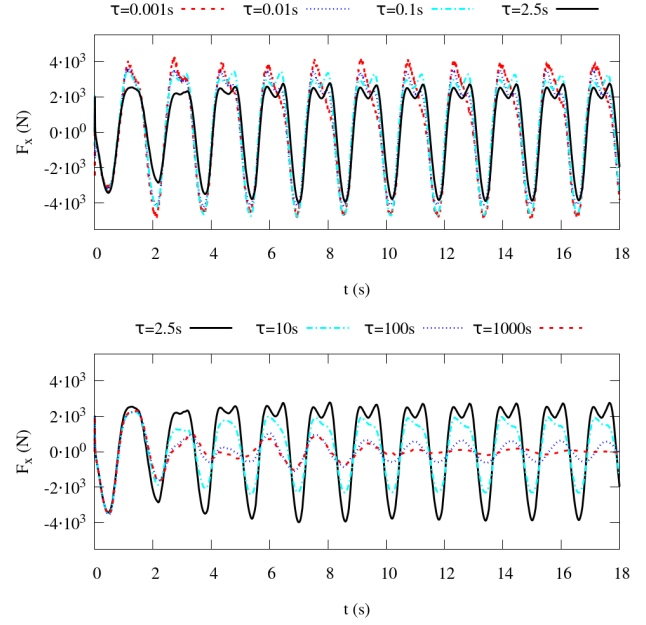


Figure 13: Force component in x -direction integrated over the pontoon surface as a function of time t for the *medium grid*; with relaxation zone thickness $x_d \approx 0.7\lambda$, power blending with exponent $n = 0.46$ and different values of relaxation parameter τ ; the analytical approach from Sect. 4 predicts an optimum of $\tau = 2.5$ s, for which a periodic solution is obtained; the further τ deviates from the theoretical optimum, the stronger are the visible influences of undesired wave reflections in the results

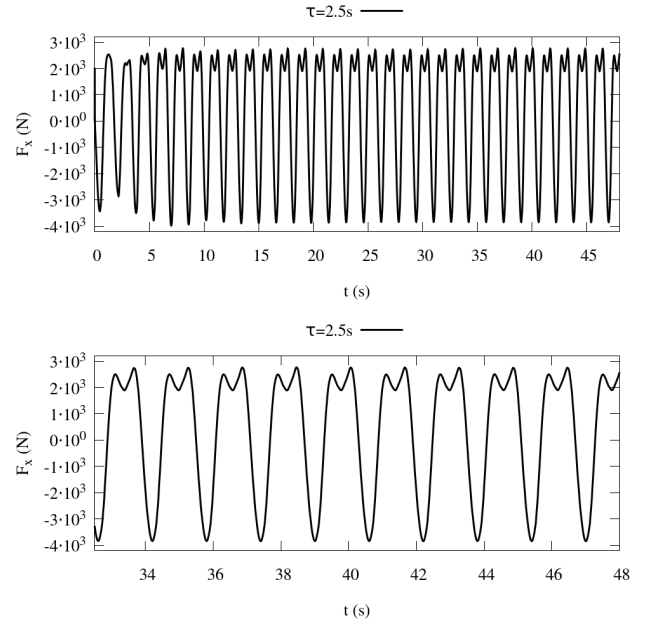


Figure 14: As Fig. 13, except for longer simulation duration; with close-to-optimum relaxation ($\tau = 2.5$ s), simulations were performed for $30T$ without noticeable accumulation of reflections

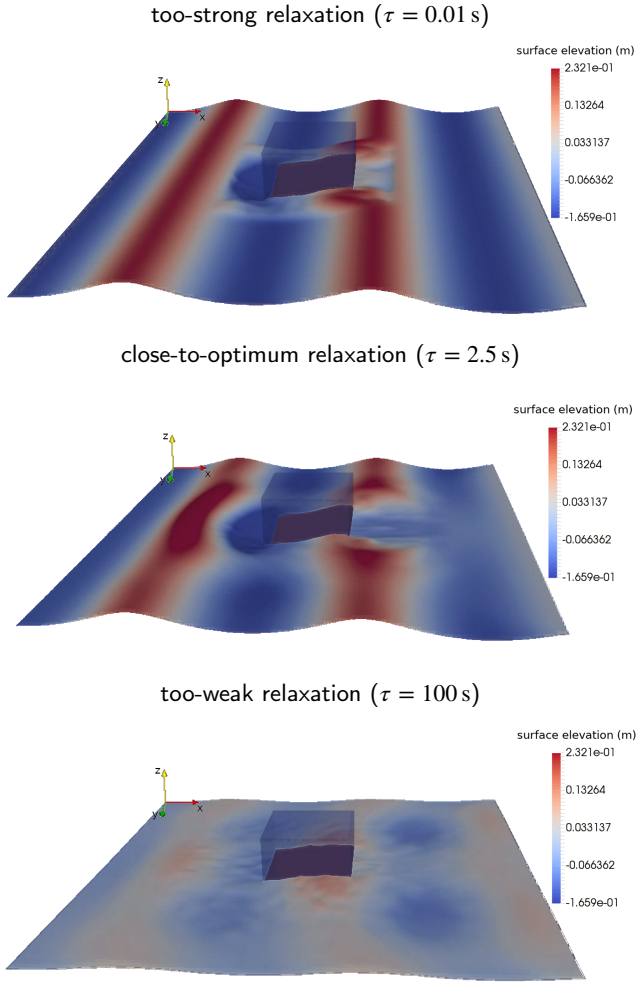


Figure 15: Simulation results for free-surface elevation at $t \approx 15$ s for different values of relaxation parameter τ ; for relaxation-zone thickness $x_d \approx 0.7\lambda$ and blending via Eq. (9) with exponent $n = 0.46$; if the relaxation is too strong (top), wave-reflection occurs near the entrance to the relaxation zone; if relaxation is too weak (bottom), the far-field wave is not sustained; for optimized relaxation-setup (middle), the waves reflected at the pontoon decay smoothly over the whole relaxation zone as intended

occurred especially for smaller-than-optimum values of relaxation parameter τ . The reason for this is that the analytical approach neglects that wave reflections due to source terms in different governing equations can have different phases and thus can partially cancel due to destructive interference. Future work will focus on considering this effect in the analytical approach, to obtain more accurate predictions of C_R .

However, already in its present form, the analytical approach predicts the relevant flow features and is sufficiently accurate to optimize the implicit relaxation zone's parameters. The analytical prediction for C_R can be considered as a close estimate of the upper-limit of the reflection coefficient C_R that will occur in the flow simulations.

How does optimizing the relaxation zone's parameters

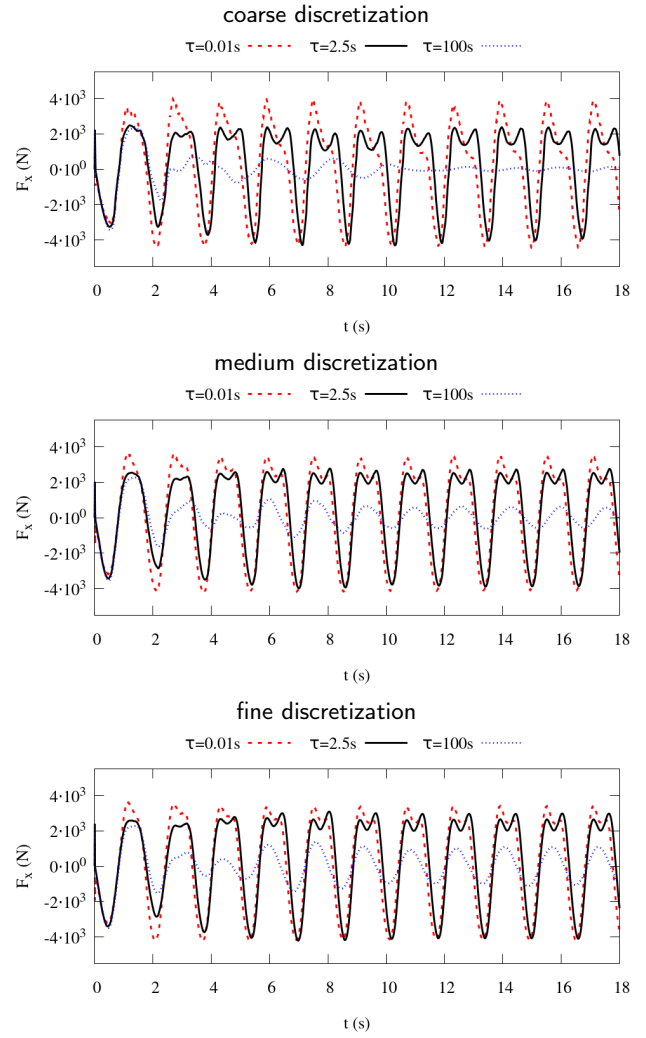


Figure 16: As Fig. 13, except for coarse, medium and fine discretization

compare to using the default settings? The default value for τ in the Naval Hydro Pack is the time-step, i.e. $\tau = \Delta t$. This is a better choice than setting τ to a constant value, because $\tau = \Delta t$ scales correctly from model to full scale and produces a favorable matrix conditioning. However, it does not coincide with the optimum τ -value: In Fig. 4 $\tau = \Delta t$ is up to two and in Fig. 11 even up to four orders of magnitude smaller than optimal. Moreover, reflection increases if the time-step is refined, thus in a discretization-dependence study the results may not converge. It is therefore both more effective and more reliable to optimize the relaxation zone's parameters.

Optimizing the relaxation zone's parameters τ , x_d and $b(\mathbf{x})$ also enables the use of thinner relaxation zones. With correct optimization, already a zone thickness of $0.5\lambda \leq x_d \leq 1.0\lambda$ (depending on the intended reflection coefficient C_R) minimizes undesired wave reflections satisfactorily. With default settings, an at least two to three times larger zone thickness would be required to obtain the same reduction of undesired reflections (cf. Sect. 6.5). Considering that typical values for zone thickness x_d in literature are $1\lambda \leq$

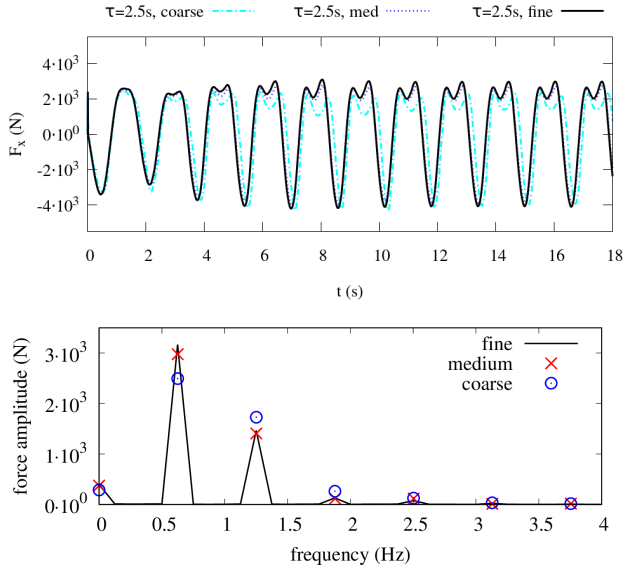


Figure 17: Top: As Fig. 13, except for close-to-optimum relaxation parameter τ on coarse, medium and fine discretization; bottom: force amplitude as a function of frequency for FFT-analysis of the curves from the upper plot during time interval $10 \leq t \leq 18$ s; between the coarse and fine discretization, all differences are < 660 N, which corresponds to over 20% of the first harmonic's amplitude; between the medium and fine discretization, all differences are < 190 N, which corresponds to $\approx 6\%$ of the first harmonic's amplitude, so already the medium discretization is considered acceptable for the present purposes

$x_d \leq 4\lambda$ (cf. Chen et al., 2019), the computational effort can typically be reduced significantly when the relaxation zone's parameters are optimized.

The necessity of optimizing the case-dependent parameters of implicit relaxation zones becomes apparent when considering that, from short ocean waves to tidal waves, the wave period T and correspondingly the optimum value for relaxation parameter τ can vary by factor 10^4 or more, while variation of zone thickness x_d and blending function $b(\mathbf{x})$ can introduce a further variation by factor of 10^3 or more. Consequently, the optimum τ -value can vary by 7 orders of magnitude for various marine applications.

It was shown that implicit relaxation zones can be considered as a special-case of forcing zones. Therefore, findings obtained for forcing zones can be applied to implicit relaxation zones and vice versa, following the procedure outlined in this work. This is supported by the findings from Sect. 6.3, which indicate that, when correctly optimized, forcing zones and implicit relaxation zones produce similar reduction of undesired wave reflections. Thus, the present results do not point in favor of one method over the other, rather the method available in one's flow solver should be used.

Future research will focus on extending the analytical approach from Perić and Abdel-Maksoud (2018) to explicit relaxation zones. If this is achieved, a unified formulation for

the analytical description of all approaches for wave-generation and wave-damping based on domain-internal source terms has been obtained.

9. Conclusion

An analytical approach was proposed for optimizing the case-dependent parameters of implicit relaxation zones before performing the flow simulations. A computer program that evaluates the analytical approach has been published as free software, to facilitate use of the approach in engineering practice.

The analytical predictions were validated against flow simulation results using two different codes, the *foam-extend* Naval Hydro Pack and Siemens STAR-CCM+. Flow simulations of free-surface wave propagation with implicit relaxation zones were performed for a wide range of settings for the relaxation zone's parameters, for relaxation towards different reference solutions, under shallow-water and deep-water conditions, for different wave periods, for both linear and nonlinear waves with up to 66% of breaking steepness, and for both 2D- and complex 3D-flow problems.

The analytical predictions for the optimum values of the case-dependent parameters matched closely with the corresponding simulation results. When the implicit relaxation zones were optimized as proposed, the simulation results for reflection coefficient C_R were mostly lower or equal their theoretical predictions, but never more than 3.4% larger.

Furthermore, it was demonstrated that optimizing the relaxation zone's parameters enables the use of significantly thinner zones and thus reduces the computational effort. Therefore, the proposed analytical approach can be recommended for optimizing implicit relaxation zones in engineering practice.

Acknowledgements

The study was supported by the Deutsche Forschungsgemeinschaft (DFG) with grants AB 112/11-1 and AB 112/11-2.

References

- [1] Berndt, J. C., Perić, R., Abdel-Maksoud, M., 2021. Improved Simulation of Flows with Free-Surface Waves by Optimizing the Angle Factor in the HRIC Interface-Sharpening Scheme. *J. Appl. Fl. Mech.*, 14 (3), pp. 909-920. <https://doi.org/10.47176/jafm.14.03.32062>.
- [2] Carmigniani, R. A., Violeau, D., 2018. Optimal Sponge Layer for water waves numerical models. *Ocean Eng.*, 163. <https://doi.org/10.1016/j.oceaneng.2018.05.068>.
- [3] Chen, Q., Kelly, D. M., Zang, J., 2019. On the relaxation approach for wave absorption in numerical wave tanks. *Ocean Eng.*, 187, 106210. <https://doi.org/10.1016/j.oceaneng.2019.106210>.
- [4] Choi, J., Yoon, S. B., 2009. Numerical simulations using momentum source wave-maker applied to RANS equation model. *Coastal Eng.*, 56 (10), 1043-1060. <https://doi.org/10.1016/j.coastaleng.2009.06.009>.
- [5] Choi, Y. M., Kim, Y. J., Bouscasse, B., Seng, S., Gentaz, L., Ferrant, P., 2020. Performance of different techniques of generation and absorption of free-surface waves in computational fluid dynamics. *Ocean Eng.*, 214, 107575. <https://doi.org/10.1016/j.oceaneng.2020.107575>.

- [6] Engsig-Karup, A. P., Hesthaven, J. S., Bingham, H. B., Madsen, P. A., 2006. Nodal DG-FEM solution of high-order Boussinesq-type equations. *J. Eng. Math.*, 56 (3), 351-370. <https://doi.org/10.1007/s10665-006-9064-z>.
- [7] Ferziger, J. H., Peric, M., 2020. Computational methods for fluid dynamics. Springer Nature Switzerland AG 2020, Cham, Switzerland. <https://doi.org/10.1007/978-3-319-99693-6>.
- [8] Fuhrman, D. R., Madsen, P. A., Bingham, H. B., 2006. Numerical simulation of lowest-order short-crested wave instabilities. *J. Fluid. Mech.*, 563, 415. <https://doi.org/10.1017/S0022112006001236>.
- [9] Higuera, P., 2020. Enhancing active wave absorption in RANS models. *Appl. Ocean Res.*, 94, 102000. <https://doi.org/10.1016/j.apor.2019.102000>.
- [10] Israeli, M., Orszag, S. A., 1981. Approximation of radiation boundary conditions. *J. Comput. Phys.*, 41 (1), 115-135. [https://doi.org/10.1016/0021-9991\(81\)90082-6](https://doi.org/10.1016/0021-9991(81)90082-6).
- [11] Jacobsen, N. G., Fuhrman, D. R., Fredsøe, J., 2012. A wave generation toolbox for the open-source CFD library: OpenFoam. *Int. J. Numer. Meth. Fl.*, 70 (9), 1073-1088. <https://doi.org/10.1002/flid.2726>.
- [12] Jasak, H., Vukčević, V., Gatin, I., 2015. Numerical Simulation of Wave Loads on Static Offshore Structures. In: *CFD for Wind and Tidal Offshore Turbines*, Springer Tracts in Mechanical Engineering, Cham, pp. 95-105. ISBN 978-3-319-16201-0. <http://dx.doi.org/10.1007/978-3-319-16202-7>.
- [13] Kim, J., O'Sullivan, J., Read, A., 2012. Ringing analysis of a vertical cylinder by Euler overlay method. In *Proc. OMAE2012*, Rio de Janeiro, Brazil. <https://doi.org/10.1115/OMAE2012-84091>.
- [14] Larsen, J., Dancy, H., 1983. Open boundaries in short wave simulations – a new approach. *Coast. Eng.*, 7 (3), 285-297. [https://doi.org/10.1016/0378-3839\(83\)90022-4](https://doi.org/10.1016/0378-3839(83)90022-4).
- [15] Larsen, B. E., Fuhrman, D. R., Roenby, J., 2019. Performance of interFoam on the simulation of progressive waves. *Coast. Eng. J.*, 61 (3), 380-400. <https://doi.org/10.1080/21664250.2019.1609713>.
- [16] Li, Z., Deng, G., Queutey, P., Bouscasse, B., Ducroz, G., Gentaz, L., Touzé, D. L., Ferrant, P., 2019. Comparison of wave modeling methods in CFD solvers for ocean engineering applications. *Ocean Eng.*, 188, 106237. <https://doi.org/10.1016/j.oceaneng.2019.106237>.
- [17] Madsen, P. A., Bingham, H. B., Schäffer, H. A., 2003. Boussinesq-type formulations for fully nonlinear and extremely dispersive water waves: derivation and analysis. In: *Proc. Roy. Soc. Lond. A Mat.*, 459(2033), 1075-1104. <https://doi.org/10.1098/rspa.2002.1067>.
- [18] Mani, A., 2012. Analysis and optimization of numerical sponge layers as a nonreflective boundary treatment. *J. Comput. Phys.*, 231 (2), 704-716. <https://doi.org/10.1016/j.jcp.2011.10.017>.
- [19] Mayer, S., Garapon, A., Sørensen L., 1998. A fractional step method for unsteady free-surface flow with applications to nonlinear wave dynamics. *Int. J. for Num. Meth. Fl.*, 28 (2), 293-315. [https://doi.org/10.1002/\(SICI\)1097-0363\(19980815\)28:2<293::AID-FLD719>3.0.CO;2-1](https://doi.org/10.1002/(SICI)1097-0363(19980815)28:2<293::AID-FLD719>3.0.CO;2-1).
- [20] Miquel, A. M., Kamath, A., Alagan Chella, M., Archetti, R., Bihs, H., 2018. Analysis of different methods for wave generation and absorption in a CFD-based numerical wave tank. *J. Mar. Sci. Eng.*, 6 (2), 73. <https://doi.org/10.3390/jmse6020073>.
- [21] Park, J. C., Zhu, M., Miyata, H., 1993. On the accuracy of numerical wave making techniques. *J. Soc. Naval Arch. Japan*, (173), 35-44. <https://doi.org/10.2534/jjasnaoe1968.1993.35>.
- [22] Park, J. C., Kim, M. H., Miyata, H., 1999. Fully non-linear free-surface simulations by a 3D viscous numerical wave tank. *Int. J. Numer. Meth. Fl.*, 29 (6), 685-703. [https://doi.org/10.1002/\(SICI\)1097-0363\(19990330\)29:6<685::AID-FLD807>3.0.CO;2-D](https://doi.org/10.1002/(SICI)1097-0363(19990330)29:6<685::AID-FLD807>3.0.CO;2-D).
- [23] Park, J. C., Kim, M. H., Miyata, H., 2001. Three-dimensional numerical wave tank simulations on fully nonlinear wave-current-body interactions. *J. Mar. Sci. Tech.*, 6 (2), 70-82. <https://doi.org/10.1007/s773-001-8377-2>.
- [24] Perić, R., Abdel-Maksoud, M., 2016. Reliable damping of free-surface waves in numerical simulations. *Ship Tech. Res.*, 63 (1), 1-13. <https://doi.org/10.1080/09377255.2015.1119921>.
- [25] Perić, R., Abdel-Maksoud, M., 2018. Analytical prediction of reflection coefficients for wave absorbing layers in flow simulations of regular free-surface waves. *Ocean Eng.*, 147, 132-147. <https://doi.org/10.1016/j.oceaneng.2017.10.009>.
- [26] Perić, R., 2019. Minimizing undesired wave reflection at the domain boundaries in flow simulations with forcing zones. PhD-thesis at Hamburg University of Technology, Schriftenreihe Schiffbau, 713, Hamburg, Germany. <https://doi.org/10.15480/882.2394>.
- [27] Perić, R., Abdel-Maksoud, M., 2020. Reducing Undesired Wave Reflection at Domain Boundaries in 3D Finite Volume-Based Flow Simulations via Forcing Zones. *J. Ship Res.*, 64, 1. <https://doi.org/10.5957/jsr.2020.64.1.23>.
- [28] Rienecker, M. M., Fenton, J. D., 1981. A Fourier approximation method for steady water waves. *J. Fl. Mech.*, 104, 119-137. <https://doi.org/10.1017/S0022112081002851>.
- [29] Schmitt, P., Elsaesser, B., 2015. A review of wave makers for 3D numerical simulations. In: *Marine 2015, 6th Int. Conf. on Computat. Meth. in Marine Eng.*, Rome, Italy. <http://hdl.handle.net/2117/332346>.
- [30] Schmitt, P., Windt, C., Davidson, J., Ringwood, J. V., Whittaker, T., 2019. The efficient application of an impulse source wavemaker to CFD simulations. *J. Mar. Sci. Eng.*, 7 (3), 71. <https://doi.org/10.3390/jmse7030071>.
- [31] Ursell, F., Dean, R. G., Yu, Y. S., 1960. Forced small-amplitude water waves: a comparison of theory and experiment. *J. Fl. Mech.*, 7 (01), 33-52. <https://doi.org/10.1017/S0022112060000037>.
- [32] Vukčević, V., Jasak, H., Malenica, Š., 2016a. Decomposition model for naval hydrodynamic applications, Part I: Computational method. *Ocean Eng.*, 121, 37-46. <https://doi.org/10.1016/j.oceaneng.2016.05.022>.
- [33] Vukčević, V., Jasak, H., Malenica, Š., 2016b. Decomposition model for naval hydrodynamic applications, Part II: Verification and validation. *Ocean Eng.*, 121, 76-88. <https://doi.org/10.1016/j.oceaneng.2016.05.021>.
- [34] Vukčević, V., Jasak, H., Gatin, I., 2017. Implementation of the Ghost Fluid Method for free surface flows in polyhedral Finite Volume framework. *Comp. & Fl.*, 153, 1-19. <https://doi.org/10.1016/j.compfluid.2017.05.003>.
- [35] Vyzikas, T., Deshoulières, S., Giroux, O., Barton, M., Greaves, D., 2017. Numerical study of fixed Oscillating Water Column with RANS-type two-phase CFD model. *Renewable energy*, 102, 294-305. <https://doi.org/10.1016/j.renene.2016.10.044>.
- [36] Wei, G., Kirby, J. T., Sinha, A., 1999. Generation of waves in Boussinesq models using a source function method. *Coast. Eng.*, 36 (4), 271-299. [https://doi.org/10.1016/S0378-3839\(99\)00009-5](https://doi.org/10.1016/S0378-3839(99)00009-5).
- [37] Weller, H.G., Tabor, G., Jasak, H., Fureby, C., 1998. A tensorial approach to computational continuum mechanics using object oriented techniques. *Comput. Phys.*, 12, 620-631. <https://doi.org/10.1063/1.168744>.
- [38] Windt, C., Davidson, J., Ringwood, J. V., 2018. High-fidelity numerical modelling of ocean wave energy systems: A review of computational fluid dynamics-based numerical wave tanks. *Renewable and Sustainable Energy Reviews*, 93, 610-630. <https://doi.org/10.1016/j.rser.2018.05.020>.
- [39] Windt, C., Davidson, J., Schmitt, P., Ringwood, J. V., 2019. On the assessment of numerical wave makers in CFD simulations. *J. Mar. Sci. Eng.*, 7 (2), 47. <https://doi.org/10.3390/jmse7020047>.